CrossMark

An affected core drives network integration deficits of the structural connectome in 22q11.2 deletion syndrome

František Váša[a,*], Alessandra Griffa[a,b], Elisa Scariati[c], Marie Schaer[c,d], Sébastien Urben[e], Stephan Eliez[c,1], Patric Hagmann[a,b,1]

[a]Department of Radiology, Lausanne University Hospital (CHUV) and University of Lausanne (UNIL), Lausanne, Switzerland
[b]Signal Processing Laboratory (LTS5), Ecole Polytechnique Fédérale de Lausanne (EPFL), Lausanne, Switzerland
[c]Office Médico-Pédagogique, Department of Psychiatry, University of Geneva, Geneva, Switzerland
[d]Stanford Cognitive and Systems Neuroscience Laboratory, Stanford University School of Medicine, Palo Alto, CA, USA
[e]Service Universitaire de Psychiatrie de l'Enfant et de l'Adolescent (SUPEA), Lausanne University Hospital (CHUV) and University of Lausanne (UNIL), Lausanne, Switzerland

ARTICLE INFO

ABSTRACT

Chromosome 22q11.2 deletion syndrome (22q11DS) is a genetic disease known to lead to cerebral structural alterations, which we study using the framework of the macroscopic white-matter connectome. We create weighted connectomes of 44 patients with 22q11DS and 44 healthy controls using diffusion tensor magnetic resonance imaging, and perform a weighted graph theoretical analysis. After confirming global network integration deficits in 22q11DS (previously identified using binary connectomes), we identify the spatial distribution of regions responsible for global deficits. Next, we further characterize the dysconnectivity of the deficient regions in terms of sub-network properties, and investigate their relevance with respect to clinical profiles. We define the subset of regions with decreased nodal integration (evaluated using the closeness centrality measure) as the affected core (A-core) of the 22q11DS structural connectome. A-core regions are broadly bilaterally symmetric and consist of numerous network hubs — chiefly parietal and frontal cortical, as well as subcortical regions. Using a simulated lesion approach, we demonstrate that these core regions and their connections are particularly important to efficient network communication. Moreover, these regions are generally densely connected, but less so in 22q11DS. These specific disturbances are associated to a rerouting of shortest network paths that circumvent the A-core in 22q11DS, "de-centralizing" the network. Finally, the efficiency and mean connectivity strength of an orbito-frontal/cingulate circuit, included in the affected regions, correlate negatively with the extent of negative symptoms in 22q11DS patients, revealing the clinical relevance of present findings. The identified A-core overlaps numerous regions previously identified as affected in 22q11DS as well as in schizophrenia, which approximately 30–40% of 22q11DS patients develop.

1. Introduction

Chromosome 22q11.2 deletion syndrome (22q11DS) is a genetic disease affecting 1 in 4000 live births (Scambler, 2000), and generally caused by a 1.5–3 megabase deletion on the long arm of chromosome 22 (Lindsay et al., 1995). As approximately 30–40% of 22q11DS patients develop schizophrenia spectrum disorders during adulthood and even more will experience psychotic symptoms during their lifetime (Murphy et al., 1999; Monks et al., 2014; Schneider et al., 2014a), the 22q11.2 microdeletion has become an established genetic model for schizophrenia spectrum disorders.

Patients with 22q11DS exhibit overall reductions in brain volume and morphological abnormalities. While gray matter alterations include loss of volume (Shashi et al., 2010), cortical thickness (Bearden et al., 2009; Jalbrzikowski et al., 2013) and gyrification (Schaer et al., 2006, 2009), white matter deficits appear both more extensive and more diffuse (Barnea-Goraly et al., 2003; Simon et al., 2005). Specifically, volumetric analyses reported decreases in white matter volume in parietal, temporal (Kates et al., 2001) and frontal lobes (Campbell et al., 2006). Moreover, numerous studies used diffusion tensor imaging (DTI) to report deficits in white matter integrity in the same regions (Barnea-Goraly et al., 2003; Simon et al., 2008; Sundram et al., 2010; Kikinis et al., 2012; Jalbrzikowski et al., 2014), in the corpus callosum and midline structures (Simon et al., 2005), in tracts to and from all cerebral lobes (Radoeva et al., 2012) as well as within and between limbic structures and fronto-temporal regions (Ottet et al., 2013a). Together with gray matter abnormalities, these extensive, diffuse white matter

alterations may be responsible for disruptions in brain function (Debbané et al., 2012; Rihs et al., 2013; Scariati et al., 2014; Schreiner et al., 2014; Tomescu et al., 2014) and cognitive deficits (Glaser et al., 2007; Dufour et al., 2008).

Diffuse and distributed diseases such as 22q11DS are suited for analysis using the framework of the structural magnetic resonance connectome, a holistic description of the brain's macroscopic connectivity (Hagmann, 2005; Sporns et al., 2005). A structural magnetic resonance connectome is a complex network, where nodes correspond to gray matter regions, while edges capture white matter connectivity between them. In binary networks, edges only indicate the presence of connections between regions. Conversely, weighted networks capture the relative importance of network connections. Various magnetic resonance measures of diffusivity or myelination can be used to quantify edge importance, reflecting diverse properties of the underlying white matter substrate (Hagmann et al., 2010).

The mathematical framework of graph theory can be applied to connectomes to characterize organizational principles of brain network connectivity in health and their breakdown in disease (Hagmann et al. 2008; Bullmore and Sporns, 2009). This framework has been applied to numerous pathologies (Griffa et al., 2013; Rubinov and Bullmore, 2013), including schizophrenia (van den Heuvel et al., 2010; Zalesky et al., 2011; Fornito et al., 2012; Wang et al., 2012a; van den Heuvel and Fornito, 2014) and 22q11DS (Ottet et al., 2013b).

The first study to apply graph theory to binary connectomes of 22q11DS patients reported deficits in topological integration and an involvement of important "hub" nodes in the disease. Moreover, it demonstrated associations between individual hallucination scores and the local efficiency of several regions hypothesized to be involved in causing hallucinations (Ottet et al., 2013b). However, the subset of regions responsible for global differences in integration was not pinpointed, or studied.

Graph theoretical measures of global connectivity can be sensitive to connectivity alterations in disease, although their specificity is impeded by the potential of different diseases to affect global brain topology in similar ways (Griffa et al., 2013; Rubinov and Bullmore, 2013). At the local level, disease-specific dysconnectivity has been studied using nodal graph-theoretical measures (e.g., van den Heuvel et al., 2010; Ottet et al., 2013b; see also Griffa et al., 2013), as well as statistical methods designed to identify network components (Zalesky et al., 2010; Meskaldji et al., 2011) or individual edges and nodes (Meskaldji et al., 2015) with reduced connectivity strength. However, the dysconnectivity of sub-networks responsible for deficits in higher-order network properties such as integration or segregation has, until recently (Griffa et al., 2015), not been studied.

In this study, we use weighted network analysis to confirm findings of deficits in global integration in 22q11DS, previously reported in an overlapping sample of participants using binary connectomes (Ottet et al., 2013b). In addition, we extend previous findings of 22q11DS dysconnectivity by identifying and studying the spatial distribution of regions driving the global integration differences, referred to as the "affected core" (A-core). We demonstrate that these core regions and their connections are particularly important to efficient network communication, describe their role in disrupting communication efficiency in the 22q11DS connectome and identify network alterations related to negative symptoms in 22q11DS.

2. Methods

2.1. Participants

Forty-four participants with 22q11DS aged between 13.1 and 31.5 years (median(inter-quartile range) = 18.2(5.9) years) participated in the study. The chromosome 22q11.2 deletion was confirmed by analysis of a blood sample with the Quantitative Fluorescent Polymerase Chain Reaction.

Forty-four healthy participants aged between 13.1 and 30.4 years (median(inter-quartile range) = 17.8(6.2) years) served as controls. None of the control participants had a history of psychiatric or neurological disorders. Subjects were matched for age (two-tailed Wilcoxon rank-sum test (WRST), p = 0.65) and gender, each group consisting of 23 females and 21 males.

Participants' IQ was assessed using Wechsler intelligence scales — WISC-III for children under 17 years (Wechsler, 1991) and WAIS-III for older participants (Wechsler, 1997). There were significant differences in full-scale IQ between 22q11DS patients (median(inter-quartile range) = 69.5(17)) and healthy participants (median(inter-quartile range) = 107.5(18)) (two-tailed WRST, p < 0.001).

22q11DS patients completed the Schizotypal Personality Questionnaire (SPQ) (Raine, 1991), which assesses the presence of symptoms from positive (e.g., hallucination or delusion), negative (e.g., social withdrawal or blunted affect) and disorganized (e.g., odd speech and behavior) dimensions. The medians(inter-quartile ranges) on the SPQ were respectively: Total Score — 20(27.5), Positive — 6(12), Negative — 5(10) and Disorganized — 9(6). Moreover, the presence of psychiatric disorders was evaluated using the Diagnostic Interview for Children and Adolescents — Revised (DICA-R; Reich, 2000) for adolescents under 18 years, and using the Structured Clinical Interview for DSM-IV axis I disorders (SCID-I; First et al., 1996). Of the sample of 44 22q11DS patients, 7 were diagnosed with psychosis (15.9%) and 2 with schizophrenia (4.6%).

At the time of testing, 17 (38.6%) patients were receiving psychotropic medication: 7 (15.9%) were on methylphenidate, 6 (13.6%) on antidepressants, 5 (11.4%) on antipsychotics, 4 (9.1%) on anticonvulsants and 1 (2.3%) on anxiolytics.

Written informed consent was obtained from all participants or their parents. The institutional review board of Geneva University School of Medicine approved the study protocol. Of the present 88 participants, 56 (63.6%) were included in a related recent study by Ottet et al. (2013b). The present sample also overlaps other (less directly relevant) recent studies on magnetic resonance imaging structural or functional connectivity in 22q11DS. Specifically, these are studies on structural connectivity (without graph-theoretical analysis) (Ottet et al., 2013a), resting-state functional connectivity (Debbané et al., 2012; Scariati et al., 2014) and structural and functional connectivity within the default mode network (Padula et al., 2015). For detailed quantitative information on sample overlaps, see supplementary table S1.

2.2. Image acquisition and preprocessing

Magnetic resonance imaging (MRI) was performed using a Siemens 3T MRI scanner, including an anatomical T1-weighted scan and a DTI scan (30 directions, maximum b-value 1000 s/mm^2). Individual connectomes were created using the Connectome Mapping ToolKit (Daducci et al., 2012), which combines several MRI processing programs into an integrated pipeline. First, T1-weighted volumes were registered to DTI data (Jenkinson et al., 2002). FreeSurfer was applied to registered T1-weighted volumes to remove non-brain tissue and segment remaining tissue into gray and white matter (Fischl et al., 2002). Subsequently, gray matter was parcellated into 82 cortical and subcortical regions of interest (ROIs). DTI data was realigned and corrected for effects of head motion (Jenkinson et al., 2002). Next, deterministic streamline tractography was used within white matter to reconstruct macroscopic white matter tracts (Wang et al., 2007). Finally, overlap between streamlines and the ROI mask enabled the creation of individual structural connectomes. Acquisition and preprocessing details are described in the supplementary information.

2.3. Weighted connectome creation

As there is currently no consensus on how best to weight connectomes, we used several connectome weightings, to ensure

robustness of our findings. The main weighting was the streamline count, or number of streamlines connecting two ROIs. Further, we used streamline density, which takes into account variability in ROI size by normalizing the streamline count between two ROIs by their mean surface area, here normalized by total cortical area (Hagmann et al., 2008). Finally, we weighted the streamline count between two ROIs by the inverse average apparent diffusion coefficient (ADC) along the corresponding white matter tract, indicative of myelination level, axonal packing or axonal integrity (Beaulieu, 2002). Streamline count, streamline density and average ADC have recently been shown to correlate to invasive measures of tract importance in the macaque, supporting their utility in weighting macroscopic white-matter connectomes in non-invasive diffusion imaging studies in humans (van den Heuvel et al., 2015). Weight definition details are reported in the supplementary information. All results reported in the results section refer to the streamline count weight definition. Results obtained using streamline density and inverse ADC weights are qualitatively consistent, and are reported in the supplementary information.

2.4. Network analysis

Connectome topology was characterized in Matlab (mathworks.com), using the Brain Connectivity Toolbox (Rubinov and Sporns, 2010) and customized code.

We evaluated two measures of global integration — the characteristic path length and global efficiency, or average inverse shortest path length, both of which quantify the ease of communication between distant brain areas (Latora and Marchiori, 2001). We also assessed segregation using transitivity, which is the ratio between pairs and triplets of nodes within the network (Newman, 2010). Between-group differences in global graph-theoretical metrics were assessed using two-tailed WRSTs.

Following our results and those of Ottet et al. (2013b), indicating a decrease in integration in 22q11DS, we thereafter focused on regions driving global integration deficits. Thus, we identified the spatial distribution of regions responsible for the difference in global integration, by comparing distributions in local measures analogous to global ones using two-tailed WRSTs and correcting for multiple comparisons using the false discovery rate (FDR) (Benjamini and Hochberg, 1995). For local differences in integration we used the closeness centrality, which is the inverse of the sum of topological distances between a node and all other nodes in the network. We designate regions with decreased closeness centrality in 22q11DS, and edges connecting them, as the "affected core" — hereafter referred to as A-core. For completeness, we have repeated our analysis using the local integration measures of nodal path length and nodal efficiency, which bear similarities and differences to closeness centrality. The results obtained using these measures are located and discussed in the supplementary information.

Subsequently, we evaluated several other local topological measures, which describe the importance of individual nodes. These include the degree, a count of the number of edges connected to a node, and the strength, or sum of these edges' weights. Furthermore, we evaluated nodal betweenness centrality, which quantifies the fraction of shortest topological paths in the network that traverse a given node, and the clustering coefficient and local efficiency, which quantify the connectivity among a node's neighbors (Latora and Marchiori, 2001).

2.5. Affected core properties

A number of diseases, including 22q11DS, have been shown to involve connectome hubs — particularly important regions of the network (Lo et al., 2010; Achard et al., 2012; Ottet et al., 2013b; Crossley et al., 2014). To qualitatively assess the topological importance of A-core regions within the healthy network, we ranked nodes in descending order according to each of their average nodal properties in control participants, and highlighted A-core regions.

Subsequently, we compared effects of simulated A-core-targeted lesions and random lesions against the entire network (Kaiser et al., 2007; Alstott et al., 2009). First, we removed all edges interconnecting A-core regions from each participant's connectome, and evaluated the global efficiency of the lesioned network. Then, we assessed the statistical significance of the result using Z-scores, evaluated relative to reference distributions of global efficiencies following 1000 random lesions of an equal number of randomly selected edges each subject's connectome.

Next, we assessed whether the mutual connectivity strength of A-core regions is different than expected based on their degree alone. First, we evaluated the mean strength of within-A-core edges for each subject. Then, we computed Z-scores of the result relative to reference distributions of average weights of the same edges, within 1000 weight-randomized connectomes with preserved binary topology.

In both permutation approaches described above, we evaluated differences between Z-score distributions of 22q11DS patients and healthy controls using one-tailed WRSTs. Considering that A-core regions are by definition affected in 22q11DS, we expected lesions of A-core edges to have a lesser impact on the global efficiency of 22q11DS patients than controls, and the interconnectivity strength of A-core regions, not accounted for by degree, to be lower in 22q11DS patients than controls.

Moreover, defining the A-core sub-network enables discriminating "core" edges, which interconnect A-core regions, "feeder" edges, which connect A-core regions to remaining peripheral ones, and "peripheral" edges, which interconnect peripheral regions. To assess whether different edge types are differentially affected in 22q11DS, we compared connectivity within these three edge classes between both groups, using two edge-specific measures — their average weight and their average edge betweenness centrality, which in analogy to nodal betweenness centrality quantifies the fraction of shortest network paths which traverse a given edge (Newman, 2010). We assessed differences in these measures using two-tailed WRSTs.

2.6. Relation to symptomatology

Finally, we assessed potential impacts of network dysconnectivity on symptomatology in 22q11DS by evaluating Spearman correlations between the average strength and global efficiency of a subset of A-core nodes (see supplementary information for details regarding included regions) and SPQ scores (total, positive, negative, disorganized). The selection of the subset of A-core nodes was based on previous studies (see Section 3.4 for details). We repeated these correlations while controlling for age and IQ.

3. Results

All results reported below refer to the streamline count definition of edge weights. Results obtained using edge weight definitions of streamline density and streamline count weighted by inverse ADC are qualitatively consistent, and are reported in the supplementary information. Medians and first and third quartiles (Q1,Q3) of all distributions compared using WRSTs are located in supplementary table S2.

3.1. Global network measures

Connectomes of 22q11DS patients presented significantly decreased global integration, demonstrating both increased characteristic path length (p = 0.0039) and decreased global efficiency (p = 0.019) (Fig. 1A). Furthermore, connectomes of 22q11DS patients possessed lower global segregation, evaluated using transitivity (p = 0.032) (supplementary figure S1A).

Further, we tested differences in global properties using local measures averaged over all nodes for each subject. This confirmed a decrease in integration, identified by node-averaged closeness centrality (p = 0.0058) (Fig. 1B). However, node-averaged local segregation measures failed to confirm the global segregation difference, both for the clustering
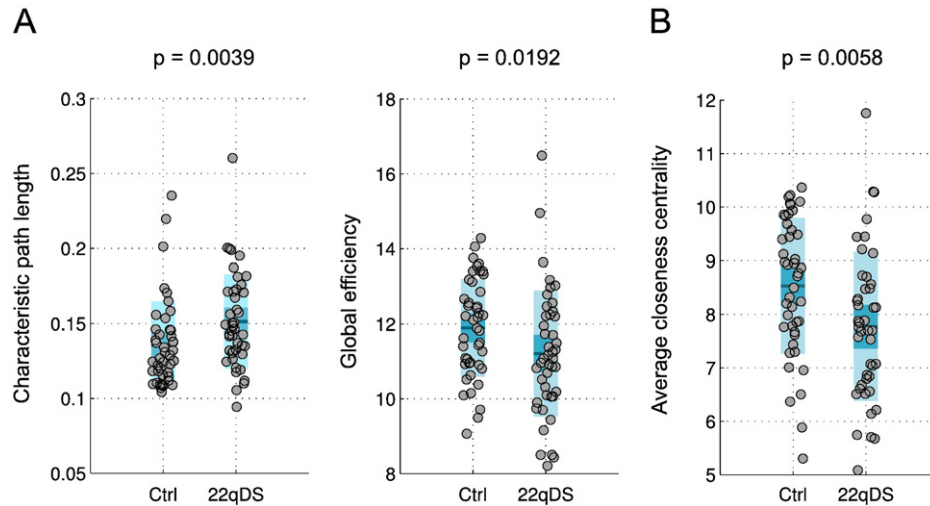
Fig. 1. Differences in global integration between healthy controls and 22q11DS patients, assessed using: (A) global measures, the characteristic path length and global efficiency, and (B) a node-averaged local measure, closeness centrality. p-values refer to two-tailed Wilcoxon rank-sum tests.

coefficient ($p = 1$) and local efficiency ($p = 0.67$) (supplementary figure S1B).

Importantly, these topological differences could not be explained by a potential difference in the number of reconstructed streamlines ($p = 0.32$) or in edge density ($p = 0.95$) between the two groups (two-tailed WRSTs).

3.2. Identification of the 22q11DS affected core

Based on the robust integration deficit results, we investigated the spatial distribution of regions driving the global group difference using closeness centrality. When averaged over all nodes, this measure is highly correlated to global efficiency, and highly inversely correlated to the characteristic path length (supplementary figure S2). A total of 31 regions presented decreased closeness centrality in 22q11DS (FDR-corrected two-tailed WRST; $p < 0.05$), which were defined as the affected core, or

A-core (Fig. 2). No regions with increased closeness centrality in 22q11DS were found.

Affected regions are broadly bilaterally symmetric. Regions with bilaterally decreased closeness centrality include superior frontal and orbitofrontal cortex, precentral gyrus, superior and inferior parietal lobules, precuneus and entorhinal cortex as well as caudate nucleus, putamen, thalamus and hippocampus. On the left side, the cingulate cortex, parahippocampal gyrus, cuneus and amygdala are also affected whereas on the right side the pericalcarine cortex and pallidum are involved. For a list of all affected regions and associated raw and FDR-corrected p-values, see supplementary table S3.

For all patients and controls, A-core nodes form a single connected component, which justifies considering them as a sub-network of the connectome. Further, the fact that these regions are driving the global integration deficit is highlighted by evaluating differences in integration between patients and controls within the A-core only. Both
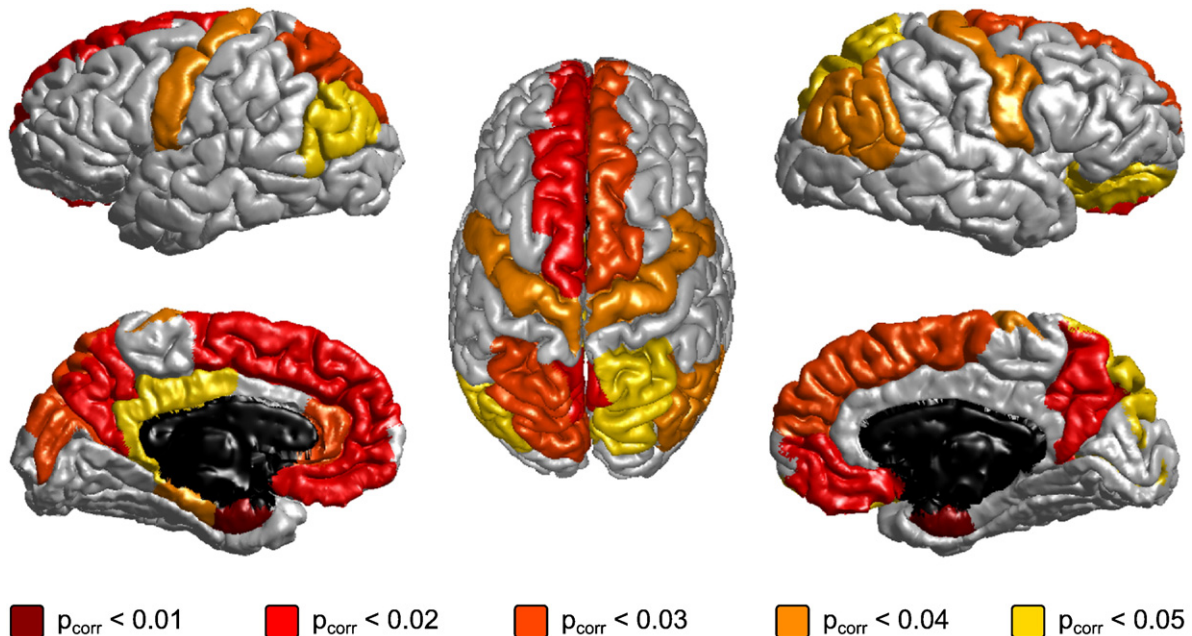
Fig. 2. The affected core, or A-core, of regions with reduced closeness centrality in 22q11DS. Regions are color-coded according to p-values from two-tailed Wilcoxon rank-sum tests, corrected for multiple comparisons using the false discovery rate (FDR). Only cortical regions are visualized; a list of all A-core regions, with associated raw and FDR-corrected p-values, is found in supplementary table S3.

characteristic path length ($p = 2.9 \cdot 10^{-6}$) and global efficiency ($p = 4.1 \cdot 10^{-5}$) show strongly significant decreases in integration in 22q11DS (supplementary figure S3).

Although differences in global segregation were not significant when using average nodal measures, for the sake of completeness we assessed local differences in segregation by comparing nodal clustering coefficients between the two groups using FDR-corrected two-tailed WRSTs. For results, see the supplementary information.

3.3. Affected core properties

A-core nodes are largely hubs of the healthy network, featuring among highest-ranked nodes for node centrality and path centrality measures evaluated on control connectomes. Considering node centrality measures, 16 of the 20 highest degree nodes and 15 of the 20 highest strength nodes are part of the A-core (Fig. 3A). Concerning path centrality, 13 of the 20 highest closeness centrality nodes and 18 of the 20 highest betweenness centrality nodes are A-core members (Fig. 3B). When considering node clustering, A-core nodes are distributed relatively evenly amongst the ranking (Fig. 3C). For numerical details on the rankings of all regions by each nodal property, see supplementary table S4.

When comparing effects of A-core-targeted and random lesions on network efficiency, a lesion of A-core edges disrupts global network efficiency far more than randomly located lesions of equal magnitude (Fig. 4A). Z-scores of global efficiency after targeted A-core lesions, relative to reference distributions of global efficiencies following random lesions, were significantly smaller than zero in both healthy controls and 22q11DS patients (both $p < 10^{-10}$). Notably, lesions of deficient edges are less harmful to network integrity than lesions of healthy edges, as underlined by a significantly lesser impact of targeted lesions on efficiency of 22q11DS connectomes ($p = 0.00067$).

While A-core nodes are mostly hubs, their mutual connectivity strength cannot be accounted for by their high degree alone (Fig. 4B). Z-scores of mean within-A-core strength, relative to reference distributions of mean within-A-core strength, within connectomes with preserved binary topology but randomized edge weights, were greater than zero in both healthy controls and 22q11DS patients (both $p < 10^{-10}$). Thus, A-core nodes are more strongly interconnected than expected on the basis of their high degree alone, in both groups. However, this effect is significantly lower in 22q11DS patients ($p = 0.00040$).

Finally, distinguishing A-core and peripheral nodes enables differentiating three classes of edges — core, feeder and peripheral, which provide specificity in comparing average weight and edge betweenness centrality between the two groups. In 22q11DS patients, average

connection weight was reduced within A-core edges ($p = 0.0025$), but not within feeder edges ($p = 0.48$) or peripheral edges ($p = 0.86$). In a post-hoc analysis, we unraveled the contributions to this effect by the total edge weight and by the number of edges. While the total number of edges within each class did not significantly differ between groups for A-core edges ($p = 0.20$), feeder edges ($p = 0.93$) or peripheral edges ($p = 0.46$), the total edge weight was significantly decreased in 22q11DS for A-core edges ($p = 0.00018$) but not for feeder edges ($p = 0.99$) or peripheral edges ($p = 0.20$). Moreover, in 22q11DS, average edge betweenness centrality was decreased in A-core edges ($p = 0.0012$) and increased in feeder edges ($p = 0.0044$) and peripheral edges ($p = 0.0049$) (Fig. 5).

3.4. Relation to symptomatology

Regarding the important role played by orbito-frontal and cingulate cortices in the emergence of negative symptoms (Wolkin et al., 2003; Ohtani et al., 2014), we computed Spearman correlations between connectivity of this circuit, substantially overlapping the A-core, and SPQ scores, expecting significant correlations to negative symptoms only. As hypothesized, significant negative correlations were present between the strength ($\rho = -0.37$, $p = 0.012$) and global efficiency ($\rho = -0.30$, $p = 0.048$) of this circuit and the SPQ negative symptom scale. No significant correlations were present with other SPQ items — total, positive or disorganized (supplementary table S6). When controlling for age and IQ, there is a significant correlation of negative symptoms with strength ($\rho = -0.38$, $p = 0.011$) and a trend-level correlation with efficiency ($\rho = -0.28$, $p = 0.069$). For alternative edge weight definitions, both correlations are significant both before and after correcting for age and IQ (supplementary table S6). Although correlations between connectivity and SPQ scores are qualitatively independent of age and IQ and consistent across edge weight definitions, they have not been corrected for multiple comparisons and should thus be considered as preliminary.

3.5. Effects of age and IQ

To verify that differences in connectivity between healthy participants and 22q11DS patients are not driven by significant IQ differences between the two cohorts, or influenced by the wide age range of our participant sample, we evaluated post-hoc Spearman correlations between several connectivity measures and both IQ and age. The connectivity measures included both global and within-A-core integration (characteristic path length and global efficiency), as well as the average strength of within-A-core, feeder and peripheral edges (for definition of these edge classes, see Section 2.5 or Fig. 5). None of the correlations
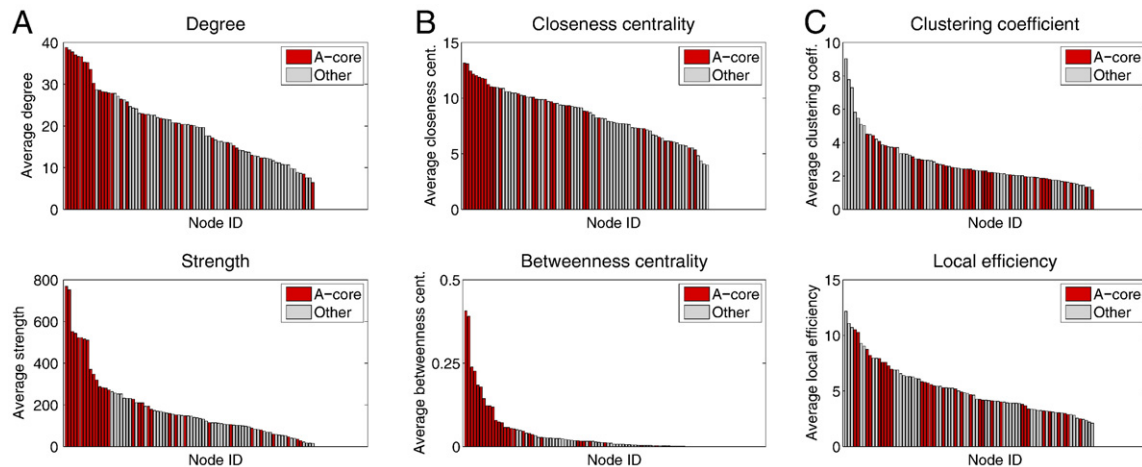
Fig. 3. Ranking of nodes by average nodal property in control subjects, with A-core regions highlighted in red. (A) Nodal centrality measures, (B) path centrality measures and (C) clustering measures. For numerical details on the rankings of all regions by each nodal property, see supplementary table S4.
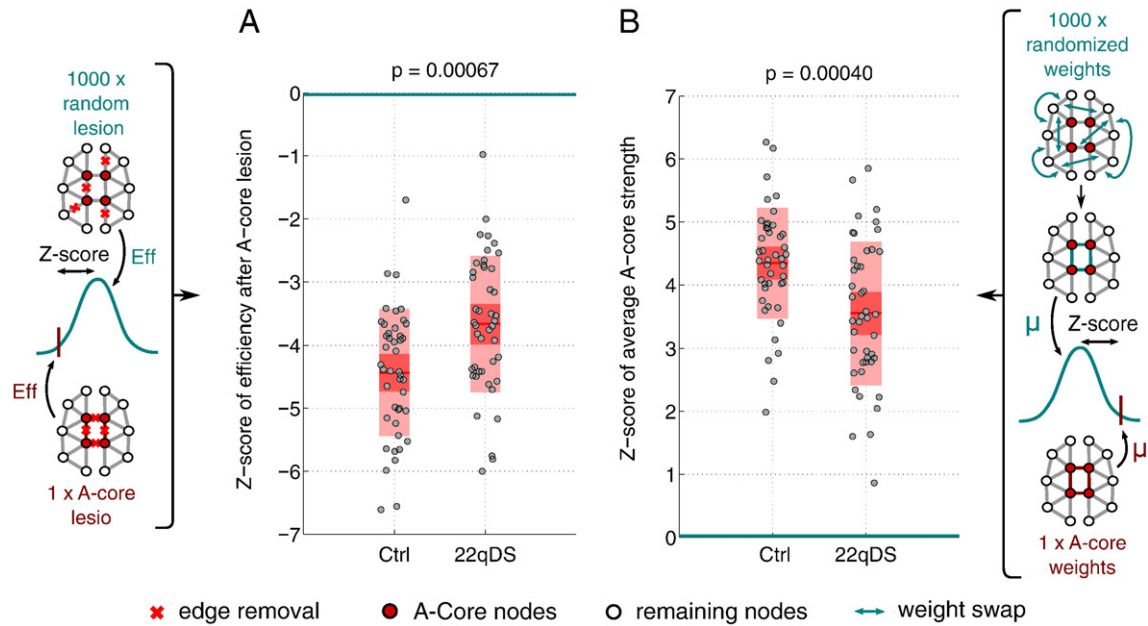
Fig. 4. Z-scores of control subjects and 22q11DS patients, obtained using permutation methods. (A) Z-scores of global network efficiencies after targeted removal of all within-A-core edges, relative to reference distributions of global efficiencies of 1000 networks where an equal number of randomly selected edges was lesioned for each subject. (B) Z-scores of average A-core strength, relative to reference distributions of average A-core strength in 1000 weight-randomized connectomes with preserved binary topology. p-values refer to one-tailed Wilcoxon rank-sum tests.

were significant, in patients or controls (supplementary table S5), providing evidence for the independence of our results on these potential confounding factors.

4. Discussion

Present weighted network results confirm integration deficits previously reported in 22q11DS using binary connectomes (Ottet et al., 2013b), and further extend previous analyses by identifying the spatial distribution of affected regions driving global effects — the A-core, which consists chiefly of densely interconnected hubs, critical for efficient network integration. These specific disturbances are associated to a rerouting of shortest network paths in 22q11DS, "de-centralizing" the network, and circumventing the A-core. Finally, connectivity of an orbito-frontal/cingulate circuit, overlapping the A-core, correlates with negative symptoms in 22q11DS. While segregation deficits also seem present, they appear weaker and less spatially compact, encouraging us to focus on integration insufficiencies.

While global graph theoretical measures can be sensitive to differences between patients and healthy controls, they are not sufficiently specific to characterize individual diseases, which can impact global brain topology in similar ways (Griffa et al., 2013; Rubinov and Bullmore, 2013). Localized deficits in nodal graph-theoretical properties in disease have been studied before (e.g., van den Heuvel et al., 2010; see also Griffa et al., 2013), but the sub-network interconnectivity of the affected nodes has not been described. Other statistical methods have been proposed, to identify network components (Zalesky et al., 2010; Meskaldji et al., 2011) or individual edges and nodes (Meskaldji et al., 2015) with reduced connectivity strength. Instead, the methods presented here and in Griffa et al. (2015) "extract" regions responsible for deficits in higher-order properties such as integration (as emphasized by strongly significant decreases of within-A-core integration in 22q11DS patients), and further characterize their inter-connectivity by considering them as a sub-network. By characterizing this sub-network, specifically affected in 22q11DS, we reach beyond global integration differences to extend our understanding of aberrant network connectivity in this genetic disease.

The presently identified A-core exhibits significant overlap with regions previously identified as affected in 22q11DS. Reports of deficits in corpus callosum as well as other midline structures (Simon et al., 2005; Machado et al., 2007; Bearden et al., 2009) could explain the largely bilateral integration reductions reported here. Furthermore, previous voxel-based studies reported decreases in radial diffusivity in bilateral parietal and frontal regions (Simon et al., 2008), in fractional anisotropy and axial diffusivity in the left parietal lobe (Kikinis et al., 2012) and in axial and radial diffusivity in multiple WM tracts (Jalbrzikowski et al., 2014). These DTI-derived indices are indicative of deficits in myelin and axonal integrity (Sun et al., 2006; Klawiter et al., 2011). The idea that myelin shortfalls could be responsible for presently reported alterations is supported by the fact that genes relevant to myelination are included in the 22q11.2 deletion region (Schreiner et al., 2013). The A-core also presents substantial overlap with regions recently identified as presenting reduced volume, cortical thickness, surface area and gyrification in 22q11DS (Schmitt et al., 2015).

Additionally, these alterations could also be caused by genetic or vascular abnormalities in 22q11DS. Cerebrovascular malformations have been suggested to impair brain development by altered perfusion (Shprintzen, 2000). Congenital heart disease, which is commonly associated with 22q11DS (McDonald-McGinn et al., 1999; Hay, 2007), can also affect brain structure in 22q11DS, both in gyrification (Schaer et al., 2006, 2009) and cortical volume (Schaer et al., 2010; Fountain et al., 2014). These links could either be due to shared genetic mechanisms (e.g., TBX1) affecting the development of both cardiovascular and nervous systems (Lindsay et al., 2001), or to cardiac malformations disrupting cerebral hemodynamics (Schaer et al., 2009).

Our results confirm an involvement of brain hubs in 22q11DS, shown by Ottet et al. (2013b), who reported reduced degree in hubs including bilateral precentral, superior and frontal parietal gyri as well as the hippocampus. Indeed, many A-core regions are hubs — highly connected and central nodes. Furthermore, our A-core exhibits substantial overlap with known structural cores of the healthy brain (Hagmann et al., 2008; van den Heuvel and Sporns, 2011). Our results are in line with a recent meta-analysis, demonstrating a general involvement of structural connectome hubs in the etiology of psychiatric disorders (Crossley et al., 2014).
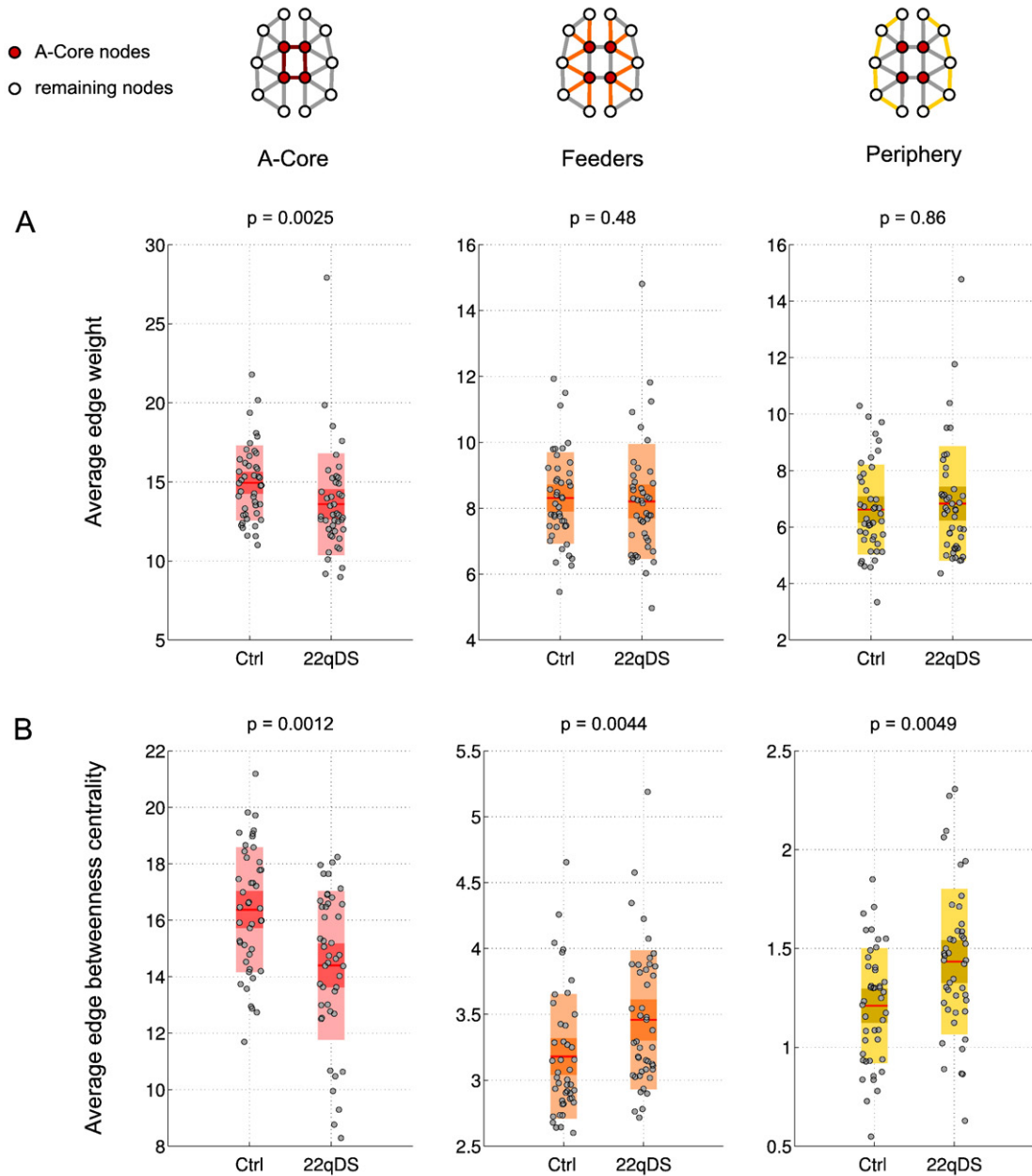
Fig. 5. Differences between healthy controls and 22q11DS patients in average properties of three classes of edges — A-core edges, interconnecting A-core nodes, feeder edges, linking A-core nodes to remaining peripheral ones and periphery edges, interconnecting peripheral nodes. (A) Average edge weight and (B) average edge betweenness centrality. p-values refer to two-tailed Wilcoxon rank-sum tests.

Having established their status as hubs, we used a simulated lesion method to demonstrate the important role of A-core nodes as well as edges interconnecting them in facilitating efficient network communication. Within each cohort, A-core-targeted lesions had greater impacts on network efficiency than random lesions of equal magnitude. Moreover, the intuitive fact that simulated lesions of deficient edges have a lesser impact on network efficiency than lesions of healthy edges confirms findings reported in a recent meta-analysis (Crossley et al., 2014).

We further characterized A-core connectivity using a permutation approach, to demonstrate that the mutual connectivity strength of A-core nodes is higher than predicted by their high degree, both in control and 22q11DS connectomes. This pattern is similar to the "rich-club" phenomenon, present in human connectomes, whereby high-degree nodes tend to possess a density of connections superior to chance (van den Heuvel and Sporns, 2011). While the rich-club approach

identifies strongly interconnected regions among high-degree nodes, we demonstrate instead that A-core regions exhibit stronger-than-expected interconnectivity, and in that respect resemble a weighted rich-club (Alstott et al., 2014). Importantly, this effect is impacted in 22q11DS, which implies a lesser concentration of strong edges within the A-core of 22q11DS patients than healthy contols.

Considering properties of A-core, feeder and peripheral edges separately confirms a lower average weight of A-core edges, although average edge weights remain unaltered for feeder and peripheral edges. This effect is driven by a decreased total weight of within-A-core edges; edge numbers do not significantly differ between groups, for either of the three edge classes. Still, the decrease of A-core edge weights in 22q11DS leads to a decrease in the number of shortest paths traversing A-core edges, as quantified by a decreased edge betweenness centrality of A-core edges. In turn, this leads to a greater proportion of shortest paths traversing feeder and peripheral edges in 22q11DS, indicating a

topological decentralization of the network through a reorganization of shortest paths in this disease.

Ultimately, the purpose of white matter structure is to support function, and thereby cognition. Thus, structural deficits reported here could be responsible for functional aberrations. Indeed, several studies report functional deficits in 22q11DS, in regions exhibiting substantial spatial overlap with the presently identified A-core. Debbané et al. (2012) identified dysconnectivity in several functional networks in 22q11DS, including superior and medial frontal gyrus as well as cingulate gyrus portions of the default mode network (DMN), and pre- and post-central gyrus portions of the sensori-motor network. Furthermore, the authors reported a correlation between atypical connectivity within the left superior frontal gyrus and prodromal symptom intensity as well as neuropsychological performance. Subsequently, Schreiner et al. (2014) confirmed DMN deficits in 22q11DS, and related them to social skills. Recently, reductions in functional connectivity between DMN nodes were explicitly shown to be driven by deficits in structural connectivity (Padula et al., 2015). Moreover, a machine learning approach applied to functional connectomes demonstrated that frontal and parietal functional connections were among the most discriminative between 22q11DS patients and healthy controls, while left anterior cingulate and precentral gyri were most discriminative between 22q11DS patients with and without psychotic symptoms (Scariati et al., 2014). The anterior cingulate cortex and dorsomedial prefrontal cortex were also implicated in altered auditory processing in 22q11DS (Rihs et al., 2013), while a further study demonstrated an association between dynamics of the salience network, which includes bilateral insula and anterior cingulate cortex, and hallucinations in 22q11DS (Tomescu et al., 2014). Generally, a model was proposed which links deficits in engagement of the above key neuro-cognitive networks to the emergence of psychiatric and neurological disorders (Menon, 2011).

In line with the status of 22q11DS as a high-risk model for schizophrenia, our results exhibit similarities with findings of dysconnectivity in this disease. Deficits in integration have been reported in schizophrenia (Zalesky et al., 2011; Wang et al., 2012a; Zhang et al., 2012; Griffa et al., 2015), with network alterations reported in fronto-temporal regions (van den Heuvel et al., 2010), a fronto-parieto-occipital network (Zalesky et al., 2011) a fronto-limbic circuit (Wang et al., 2012a) and the cerebellum (Kim et al., 2014). While our scans did not cover this important area, future work on 22q11DS connectivity should include the cerebellum, known to be affected in this disease (Campbell et al., 2006). Moreover, the "rich-club" of densely inter-connected high-degree regions is affected in schizophrenia (van den Heuvel et al., 2013; Collin et al., 2014, 2015).

One might expect more exaggerated aberrations in the connectomes of those 22q11DS patients who were diagnosed with clinical schizophrenia. However, only two of our 44 22q11DS patients have been diagnosed with schizophrenia, an insufficient number to compare to the remaining 42 non-schizophrenic 22q11DS patients, or to the healthy controls. Moreover, a previous DTI study identified no significant difference in white matter integrity, measured using fractional anisotropy and white matter volume, between 22q11DS patients with and without schizophrenia (da Silva Alves et al., 2011).

Finally, localized dysconnectivity as identified here can be associated to clinical symptoms. Negative symptoms are tightly linked to 22q11DS, being present in up to 80% of adolescents (Schneider et al., 2012, 2014b). Our finding that greater dysconnectivity in an orbito-frontal/ cingulate circuit is related to a greater expression of negative symptoms in 22q11DS confirms previous findings from schizophrenic patients (Wolkin et al., 2003; Ohtani et al., 2014), and extends them by emphasizing the role of network interactions implicated in such deficits. Indeed, orbito-frontal and cingulate cortices form a circuit hypothesized to play an important role in emotional processing (de Marco et al., 2006), decision making (Krain et al., 2006; Paulmann et al., 2010), and more generally in social behaviors (Rudebeck et al., 2008). Thus,

dysconnectivity within such a circuit could lead patients with 22q11DS to present negative symptoms, such as social withdrawal, anhedonia or blunted affect. It is crucial to understand mechanisms leading to the development of these symptoms — whereas positive symptoms can often be controlled by neuroleptics, negative symptoms are usually resistant to this treatment and cause great impairment in patients (Chien and Yip, 2013). Moreover, negative symptoms have been associated with impairments in multiple cognitive domains; in 22q11DS, they have been linked specifically to deficits in visual memory and processing speed, as well as lower functional and occupational outcome (Schneider et al., 2014b). However, negative symptoms do not appear to be caused by lower intellectual functioning in 22q11DS (Schneider et al., 2014b), in line with our results demonstrating the qualitative independence on IQ of correlations between dysconnectivity and negative symptoms. We note that while correlations between orbito-frontal/cingulate connectivity and SPQ scores are consistent for measures of strength and efficiency as well as across weight definitions, and are qualitatively independent of age and IQ, they have not been corrected for multiple comparisons and should thus be considered as preliminary, subject to confirmation in future studies.

Negative symptoms have previously been related to functional dysconnectivity in graph-theoretical studies of the functional connectome. A study constructing functional connectomes from resting-state electro-encephalogram (EEG) recordings of schizophrenic adolescents and young adults reported positive correlations between the path length and two negative symptom items from the positive and negative symptoms scale (PANSS) — loss of spontaneity (N6) and stereotypical thinking (N7) (Rubinov et al., 2009). This result was confirmed by a further task-based EEG study, reporting a significant positive correlation between the path length of the adult functional schizophrenic connectome and the negative (as well as cognitive) symptom factors from PANSS (Shim et al., 2014). Finally, these results were corroborated by a resting-state functional MRI study reporting that negative symptoms are positively correlated with path length, and negatively correlated with global efficiency, in adults with schizophrenia (Yu et al., 2011). As the path length is inversely related to network efficiency, the sign of all of these correlations suggests that lower functional integration is associated with greater negative symptoms, in line with our findings within a sub-circuit of the structural connectome. Graph theory provides a useful framework for further studies simultaneously analyzing both structural and functional connectomes; such studies will be required to disentangle the relationships between structural dysconnectivity, functional aberrations and their effect on symptomatology in 22q11DS.

Given the importance of localizing aberrant connectivity in psychiatric diseases, we have applied novel analysis methods aiming to identify sub-networks responsible for global deficits (Griffa et al., 2015) to 22q11DS diffusion imaging data, part of which had previously been explored using more standard graph-theoretical methods (Ottet et al., 2013b). Beyond its potential to provide increased sensitivity and specificity to connectivity abnormalities, moving from a global to a local characterization of dysconnectivity in disease can open up avenues for new forms of treatment, such as non-invasive transcranial magnetic or electric stimulation, which have been trialed in schizophrenia (Dougall et al., 2015). Crucially, the effectiveness of such stimulation methods depends on the structure and function of the underlying brain networks (Fox et al., 2014; Sale et al., 2015), and specifically on the (dys)connectivity of the stimulated region. Thus, the identification of deficient sub-networks, such as the presently reported affected core of the 22q11DS structural connectome, is a valuable first step towards novel locally-targeted treatment methods.

The present study has several limitations. While there is a significant difference in IQ between the two cohorts, we tried to rule out effects of this potential confounding factor. The IQ does not correlate with measures of within-A-core integration and does not qualitatively affect the correlation of orbito-frontal/cingulate connectivity with negative symptoms.

Additionally, several 22q11DS neuroimaging studies have used IQ-matched cohorts, likewise reporting white matter reductions in frontal, posterior and temporal lobes (Van Amelsvoort et al., 2001, 2004; Baker et al., 2011), largely consistent with previous studies using cohorts not matched for IQ as well as present findings. Moreover, 22q11DS patients are likely to differ in psychiatric comorbidities, such as psychosis and schizophrenia. Our results relate to the entire clinical and cognitive phenotype of 22q11DS — larger or longitudinal groups would be required to disentangle individual participant's clinical evolution or comorbidity development. Furthermore, the 22q11DS group covers a wide age range, which includes adolescence — a period where significant changes are known to occur (Giedd, 2004). Still, a close age match between our 22q11DS and control groups enables comparability between the larger cohorts, which increase statistical power. Finally, the relatively low angular resolution of DTI data used is unable to resolve crossing fibers (Hagmann et al., 2006). A dataset with higher angular resolution combined with a suitable reconstruction model would provide more anatomical detail. Still, the short acquisition time of standard DTI acquisitions is better suited to scanning clinical populations such as 22q11DS, and the reconstructed fibers present a reduced number of false positives as well as higher reproducibility (Bassett et al., 2011; Bastiani et al., 2012; Wang et al., 2012b).

In conclusion, we confirmed decreased topological integration in 22q11DS and extended our understanding of aberrant network connectivity in this genetic disease by localizing and studying the regions responsible for global deficits. The identified A-core consists of regions which in healthy connectomes are highly central and strongly connected. However, these properties are impacted in 22q11DS, along with a de-centralization of A-core regions through a re-routing of shortest network paths. Our findings suggest that like schizophrenia, which approximately 30–40% of 22q11DS patients develop (Murphy et al., 1999; Schneider et al., 2014a), 22q11DS can be considered a disease of dysconnectivity, and that this dysconnectivity is associated with negative symptomatology. In general, the methods presented here and in Griffa et al. (2015) can be extended to other diseases affecting network connectivity, as well as to functional connectomes, to identify local abnormalities driving global topological deficits.

Conflict of interest statement

The authors declare that the research was conducted in the absence of any commercial or financial relationships that could be construed as a potential conflict of interest.

Acknowledgments

Appendix A. Supplementary information

Supplementary information to this article can be found online at http://dx.doi.org/10.1016/j.nicl.2015.11.017.

References

Achard, S., Delon-Martin, C., Vértes, P.E., et al., 2012. Hubs of brain functional networks are radically reorganized in comatose patients. Proc. Natl. Acad. Sci. 109 (50), 20608–20613.

Alstott, J., Breakspear, M., Hagmann, P., Cammoun, L., Sporns, O., 2009. Modeling the impact of lesions in the human brain. PLoS Comput. Biol. 5 (6), e1000408.

Alstott, J., Panzarasa, P., Rubinov, M., Bullmore, E.T., Vértes, P., 2014. A unifying framework for measuring weighted rich clubs. Sci. Rep. 4, 7258.

Baker, K., Chaddock, C.A., Baldeweg, T., Skuse, D., 2011. Neuroanatomy in adolescents and young adults with 22q11 deletion syndrome: comparison to an IQ-matched group. NeuroImage 55 (2), 491–499.

Barnea-Goraly, N., Menon, V., Krasnow, B., Ko, A., Reiss, A., Eliez, S., 2003. Investigation of white matter structure in velocardiofacial syndrome: a diffusion tensor imaging study. Am. J. Psychiatry 160 (10), 1863–1869.

Bassett, D.S., Brown, J.A., Deshpande, V., Carlson, J.M., Grafton, S.T., 2011. Conserved and variable architecture of human white matter connectivity. NeuroImage 54 (2), 1262–1279.

Bastiani, M., Shah, N.J., Goebel, R., Roebroeck, A., 2012. Human cortical connectome reconstruction from diffusion weighted MRI: the effect of tractography algorithm. NeuroImage 62 (3), 1732–1749.

Bearden, C.E., van Erp, T.G.M., Dutton, R.A., et al., 2009. Alterations in midline cortical thickness and gyrification patterns mapped in children with 22q11.2 deletions. Cereb. Cortex 19, 115–126.

Beaulieu, C., 2002. The basis of anisotropic water diffusion in the nervous system — a technical review. NMR Biomed. 15 (7–8), 435–455.

Benjamini, Y., Hochberg, Y., 1995. Controlling the false discovery rate: a practical and powerful approach to multiple testing. J. R. Stat. Soc. Ser. B Methodol. 57 (1), 289–300.

Bullmore, E., Sporns, O., 2009. Complex brain networks: graph theoretical analysis of structural and functional systems. Nat. Rev. Neurosci. 10 (3), 186–198.

Campbell, L.E., Daly, E., Toal, F., et al., 2006. Brain and behaviour in children with 22q11.2 deletion syndrome: a volumetric and voxel-based morphometry MRI study. Brain 129 (5), 1218–1228.

Chien, W.T., Yip, A.L., 2013. Current approaches to treatments for schizophrenia spectrum disorders, part I: an overview and medical treatments. Neuropsychiatr. Dis. Treat. 9, 1311–1332.

Collin, G., Kahn, R.S., de Reus, M.A., Cahn, W., van den Heuvel, M.P., 2014. Impaired rich club connectivity in unaffected siblings of schizophrenia patients. Schizophr. Bull. 40 (2), 438–448.

Collin, G., de Nijs, J., Hulshoff Pol, H.E., Cahn, W., van den Heuvel, M.P., 2015. Connectome organization is related to longitudinal changes in general functioning, symptoms and IQ in chronic schizophrenia. Schizophr. Res. http://dx.doi.org/10.1016/j.schres.2015.03.012.

Crossley, N.A., Mechelli, A., Scott, J., et al., 2014. The hubs of the human connectome are generally implicated in the anatomy of brain disorders. Brain, http://dx.doi.org/10.1093/brain/awu132.

da Silva Alves, F., Schmitz, N., Bloemen, O., et al., 2011. White matter abnormalities in adults with 22q11 deletion syndrome with and without schizophrenia. Schizophr. Res. 132, 75–83.

Daducci, A., Gerhard, S., Griffa, A., et al., 2012. The connectome mapper: an open-source processing pipeline to map connectomes with MRI. PLoS One 7 (12), e48121.

de Marco, G., de Bonis, M., Vrignaud, P., Henry-Feugeas, M.C., Peretti, I., 2006. Changes in effective connectivity during incidental and intentional perception of fearful faces. NeuroImage 30 (3), 1030–1037.

Debbané, M., Lazouret, M., Lagioia, A., Schneider, M., Van De Ville, D., Eliez, S., 2012. Resting-state networks in adolescents with 22q11.2 deletion syndrome: associations with prodromal symptoms and executive functions. Schizophr. Res. 139 (1–3), 33–39.

Dougall, N., Maayan, N., Soares-Weiser, K., McDermott, L.M., McIntosh, A., 2015. Transcranial magnetic stimulation for schizophrenia. Schizophr. Bull. 41 (6), 1220–1222.

Dufour, F., Schaer, M., Debbané, M., Farhoumand, R., Glaser, B., Eliez, S., 2008. Cingulate gyral reductions are related to low executive functioning and psychotic symptoms in 22q11.2 deletion syndrome. Neuropsychologia 46 (12), 2986–2992.

First, M., Gibbon, M., Spitzer, R., Williams, J., 1996. Structured Clinical Interview for the DSM-IV Axis I Disorders (SCID-I). American Psychiatric Association.

Fischl, B., Salat, D.H., Busa, E., et al., 2002. Whole brain segmentation: automated labeling of neuroanatomical structures in the human brain. Neuron 33 (3), 341–355.

Fornito, A., Zalesky, A., Pantelis, C., Bullmore, E.T., 2012. Schizophrenia, neuroimaging and connectomics. NeuroImage 62 (4), 2296–2314.

Fountain, D.M., Schaer, M., Mutlu, A.K., Schneider, M., Debbané, M., Eliez, S., 2014. Congenital heart disease is associated with reduced cortical and hippocampal volume in patients with 22q11.2 deletion syndrome. Cortex 57, 128–142.

Fox, M.D., Buckner, R.L., Liu, H., Chakravarty, M.M., Lozano, A.M., Pascual-Leone, A., 2014. Resting-state networks link invasive and noninvasive brain stimulation across diverse psychiatric and neurological diseases. Proc. Natl. Acad. Sci. U. S. A. 111 (41), 4367–4375.

Giedd, J.N., 2004. Structural magnetic resonance imaging of the adolescent brain. Ann. N. Y. Acad. Sci. 1021 (1), 77–85.

Glaser, B., Schaer, M., Berney, S., Debbane, M., Vuilleumier, P., Eliez, S., 2007. Structural changes to the fusiform gyrus: a cerebral marker for social impairments in 22q11.2 deletion syndrome? Schizophr. Res. 96 (1–3), 82–86.

Griffa, A., Baumann, P.S., Thiran, J.-P., Hagmann, P., 2013. Structural connectomics in brain diseases. NeuroImage 80, 515–526.

Griffa, A., Baumann, P.S., Ferrari, C., et al., 2015. MR connectomics identifies a distributed subnetwork lesioned in schizophrenia. Hum. Brain Mapp. 36, 354–366.

Hagmann, P., 2005. From Diffusion MRI to Brain Connectomics. EPFL, Lausanne (141 pages. Available at: http://info-science.epfl.ch/record/33696.).

Hagmann, P., Jonasson, L., Maeder, P., Thiran, J.-P., Wedeen, V.J., Meuli, R., 2006. Understanding diffusion MR imaging techniques: from scalar diffusion-weighted imaging to diffusion tensor imaging and beyond. RadioGraphics 26 (Suppl. 1), S205–S223.

Hagmann, P., Cammoun, L., Gigandet, X., et al., 2008. Mapping the structural core of human cerebral cortex. PLoS Biol. 6 (7), e159.

Hagmann, P., Cammoun, L., Gigandet, X., et al., 2010. MR connectomics: principles and challenges. J. Neurosci. Methods 194 (1), 34–45.

Hay, B.N., 2007. Deletion 22q11: spectrum of associated disorders. Semin. Pediatr. Neurol. 14, 136–139.

Jalbrzikowski, M., Jonas, R., Senturk, D., et al., 2013. Structural abnormalities in cortical volume, thickness, and surface area in 22q11.2 microdeletion syndrome: relationship with psychotic symptoms. NeuroImage Clin. 3, 405–415.

Jalbrzikowski, M., Villalon-Reina, J.E., Karlsgodt, K.H., et al., 2014. Altered white matter microstructure is associated with social cognition and psychotic symptoms in 22q11.2 microdeletion syndrome. Front. Behav. Neurosci. 8, 393.

Jenkinson, M., Bannister, P., Brady, M., Smith, S., 2002. Improved optimization for the robust and accurate linear registration and motion correction of brain images. NeuroImage 17 (2), 825–841.

Kaiser, M., Martin, R., Andras, P., Young, M.P., 2007. Simulation of robustness against lesions of cortical networks. Eur. J. Neurosci. 25 (10), 3185–3192.

Kates, W.R., Burnette, C.P., Jabs, E.W., et al., 2001. Regional cortical white matter reductions in velocardiofacial syndrome: a volumetric MRI analysis. Biol. Psychiatry 49 (8), 677–684.

Kikinis, Z., Asami, T., Bouix, S., et al., 2012. Reduced fractional anisotropy and axial diffusivity in white matter in 22q11.2 deletion syndrome: a pilot study. Schizophr. Res. 141 (1), 35–39.

Kim, D.-J., Kent, J.S., Bolbecker, A.R., et al., 2014. Disrupted modular architecture of cerebellum in schizophrenia: a graph theoretic analysis. Schizophr. Bull. 40 (6), 1216–1226..

Klawiter, E.C., Schmidt, R.E., Trinkaus, K., et al., 2011. Radial diffusivity predicts demyelination in ex vivo multiple sclerosis spinal cords. NeuroImage 55 (4), 1454–1460.

Krain, A.L., Wilson, A.M., Arbuckle, R., Castellanos, F.X., Milham, M.P., 2006. Distinct neural mechanisms of risk and ambiguity: a meta-analysis of decision-making. NeuroImage 32 (1), 477–484.

Latora, V., Marchiori, M., 2001. Efficient behavior of small-world networks. Phys. Rev. Lett. 87 (19), 198701.

Lindsay, E.A., Goldberg, R., Jurecic, V., et al., 1995. Velo-cardio-facial syndrome: frequency and extent of 22q11 deletions. Am. J. Med. Genet. 57 (3), 514–522.

Lindsay, E.A., Vitelli, F., Su, H., et al., 2001. Tbx1 haploinsufficiency in the DiGeorge syndrome region causes aortic arch defects in mice. Nature 410, 97–101.

Lo, C.-Y., Wang, P.-N., Chou, K.-H., Wang, J., He, Y., Lin, C.-P., 2010. Diffusion tensor tractography reveals abnormal topological organization in structural cortical networks in Alzheimer's disease. J. Neurosci. 30 (50), 16876–16885.

Machado, A.M.C., Simon, T.J., Nguyen, V., et al., 2007. Corpus callosum morphology and ventricular size in chromosome 22q11.2 deletion syndrome. Brain Res. 1131, 197–210.

McDonald-McGinn, D.M., Kirschner, R., Goldmuntz, E., et al., 1999. The Philadelphia story: the 22q11.2 deletion: report on 250 patients. Genet. Couns. 10, 11–24.

Menon, V., 2011. Large-scale brain networks and psychopathology: a unifying triple network model. Trends Cogn. Sci. 15 (10), 483–506.

Meskaldji, D.E., Ottet, M.C., Cammoun, L., et al., 2011. Adaptive strategy for the statistical analysis of connectomes. PLoS One 6 (8), e23009.

Meskaldji, D.E., Vasung, L., Romascano, D., et al., 2015. Improved statistical evaluation of group differences in connectomes by screening-filtering strategy with application to study maturation of brain connections between childhood and adolescence. NeuroImage 108, 251–264.

Monks, S., Niarchou, M., Davies, A.R., et al., 2014. Further evidence for high rates of schizophrenia in 22q11.2 deletion syndrome. Schizophr. Res. 153 (1), 231–236.

Murphy, K.C., Jones, L.A., Owen, M.J., 1999. High rates of schizophrenia in adults with velo-cardio-facial syndrome. Arch. Gen. Psychiatry 56 (10), 940–945.

Newman, M., 2010. Networks: An Introduction. OUP Oxford.

Ohtani, T., Bouix, S., Hosokawa, T., et al., 2014. Abnormalities in white matter connections between orbitofrontal cortex and anterior cingulate cortex and their associations with negative symptoms in schizophrenia: A DTI study. Schizophr. Res. 157 (1), 190–197.

Ottet, M.-C., Schaer, M., Debbané, M., Thiran, J.-P., Eliez, S., 2013a. Graph theory reveals dysconnected hubs in 22q11DS and altered nodal efficiency in patients with hallucinations. Front. Hum. Neurosci. 7, 402.

Ottet, M.-C., Schaer, M., Cammoun, L., et al., 2013b. Reduced fronto-temporal and limbic connectivity in the 22q11.2 deletion syndrome: vulnerability markers for developing schizophrenia? PLoS One 8 (3), e58429.

Padula, M., Schaer, M., Scariati, E., et al., 2015. Structural and functional connectivity in the default mode network in 22q11.2 deletion syndrome. J. Neurodev. Disord. 7, 23.

Paulmann, S., Seifert, S., Kotz, S.A., 2010. Orbito-frontal lesions cause impairment during late but not early emotional prosodic processing. Soc. Neurosci. 5 (1), 59–75.

Radoeva, P.D., Coman, I.L., Antshel, K.M., et al., 2012. Atlas-based white matter analysis in individuals with velo-cardio-facial syndrome (22q11.2 deletion syndrome) and unaffected siblings. Behav. Brain Funct. 8 (1), 38.

Raine, A., 1991. The SPQ: a scale for the assessment of schizotypal personality based on DSM-III-R criteria. Schizophr. Bull. 17 (4), 555–564.

Reich, W., 2000. Diagnostic interview for children and adolescents (DICA). J. Am. Acad. Child Adolesc. Psychiatry 39, 59e66.

Rihs, T.A., Tomescu, M.I., Britz, J., et al., 2013. Altered auditory processing in frontal and left temporal cortex in 22q11.2 deletion syndrome: a group at high genetic risk for schizophrenia. Psychiatry Res. Neuroimaging 212 (2), 141–149.

Rubinov, M., Bullmore, E., 2013. Fledgling pathoconnectomics of psychiatric disorders. Trends Cogn. Sci. 17 (12), 641–647.

Rubinov, M., Sporns, O., 2010. Complex network measures of brain connectivity: uses and interpretations. NeuroImage 52 (3), 1059–1069.

Rubinov, M., Knock, S.A., Stam, C.J., et al., 2009. Small-world properties of nonlinear brain activity in schizophrenia. Hum. Brain Mapp. 30, 403–416.

Rudebeck, P.H., Bannerman, D.M., Rushworth, M.F.S., 2008. The contribution of distinct subregions of the ventromedial frontal cortex to emotion, social behavior, and decision making. Cogn. Affect. Behav. Neurosci. 8 (4), 485–497.

Sale, M.V., Mattingley, J.B., Zalesky, A., Cocchi, L., 2015. Imaging human brain networks to improve the clinical efficacy of non-invasive brain stimulation. Neurosci. Biobehav. Rev. 57, 187–198.

Scambler, P.J., 2000. The 22q11 deletion syndromes. Hum. Mol. Genet. 9 (16), 2421–2426.

Scariati, E., Schaer, M., Richiardi, J., et al., 2014. Identifying 22q11.2 deletion syndrome and psychosis using resting-state connectivity patterns. Brain Topogr. 27, 808–821.

Schaer, M., Schmitt, J.E., Glaser, B., Lazeyras, F., Delavelle, J., Eliez, S., 2006. Abnormal patterns of cortical gyrification in velo-cardio-facial syndrome (deletion 22q11.2): an MRI study. Psychiatry Res. Neuroimaging 146 (1), 1–11.

Schaer, M., Glaser, B., Bach Cuadra, M., Debbané, M., Thiran, J.P., Eliez, S., 2009. Congenital heart disease affects local gyrification in 22q11.2 deletion syndrome. Dev. Med. Child Neurol. 51, 746–753.

Schaer, M., Glaser, B., Ottet, M.C., et al., 2010. Regional cortical volumes and congenital heart disease: a MRI study in 22q11.2 deletion syndrome. J. Neurodev. Disord. 2, 224–234.

Schmitt, J.E., Vandekar, S., Yi, J., et al., 2015. Aberrant cortical morphometry in the 22q11.2 deletion syndrome. Biol. Psychiatry 78 (2), 135–143.

Schneider, M., Van der Linden, M., Glaser, B., et al., 2012. Preliminary structure and predictive value of attenuated negative symptoms in 22q11.2 deletion syndrome. Psychiatry Res. 196, 277–284.

Schneider, M., Debbané, M., Bassett, A.S., et al., 2014a. Psychiatric disorders from childhood to adulthood in 22q11.2 deletion syndrome: results from the international consortium on brain and behavior in 22q11.2 deletion syndrome. Am. J. Psychiatry 171 (6), 627–639.

Schneider, M., Van der Linden, M., Menghetti, S., Glaser, B., Debbané, M., Eliez, S., 2014b. Predominant negative symptoms in 22q11.2 deletion syndrome and their associations with cognitive functioning and functional outcome. J. Psychiatr. Res. 48, 86–93.

Schreiner, M.J., Lazaro, M.T., Jalbrzikowski, M., Bearden, C.E., 2013. Converging levels of analysis on a genomic hotspot for psychosis: insights from 22q11.2 deletion syndrome. Neuropharmacology 68, 157–173.

Schreiner, M.J., Karlsgodt, K.H., Uddin, L.Q., et al., 2014. Default mode network connectivity and reciprocal social behavior in 22q11.2 deletion syndrome. Soc. Cogn. Affect. Neurosci. 9, 1261–1267.

Shashi, V., Kwapil, T.R., Kaczorowski, J., et al., 2010. Evidence of gray matter reduction and dysfunction in chromosome 22q11.2 deletion syndrome. Psychiatry Res. Neuroimaging 181 (1), 1–8.

Shim, M., Kim, D.W., Lee, S.H., Im, C.H., 2014. Disruptions in small-world cortical functional connectivity network suring an auditory oddball paradigm task in patients with schizophrenia. Schizophr. Res. 156, 197–203.

Shprintzen, R.J., 2000. Velo-cardio-facial syndrome: a distinctive behavioral phenotype. Ment. Retard. Dev. Disabil. Res. Rev. 6, 142–147.

Simon, T.J., Ding, L., Bish, J.P., McDonald-McGinn, D.M., Zackai, E.H., Gee, J., 2005. Volumetric, connective, and morphologic changes in the brains of children with chromosome 22q11.2 deletion syndrome: an integrative study. NeuroImage 25 (1), 169–180.

Simon, T.J., Wu, Z., Avants, B., Zhang, H., Gee, J.C., Stebbins, G.T., 2008. Atypical cortical connectivity and visuospatial cognitive impairments are related in children with chromosome 22q11.2 deletion syndrome. Behav. Brain Funct. 4 (1), 25.

Sporns, O., Tononi, G., Kötter, R., 2005. The human connectome: a structural description of the human brain. PLoS Comput. Biol. 1 (4), e42.

Sun, S.-W., Liang, H.-F., Le, T.Q., Armstrong, R.C., Cross, A.H., Song, S.-K., 2006. Differential sensitivity of in vivo and ex vivo diffusion tensor imaging to evolving optic nerve injury in mice with retinal ischemia. NeuroImage 32 (3), 1195–1204.

Sundram, F., Campbell, L.E., Azuma, R., et al., 2010. White matter microstructure in 22q11 deletion syndrome: a pilot diffusion tensor imaging and voxel-based morphometry study of children and adolescents. J. Neurodev. Disord. 2 (2), 77–92.

Tomescu, M.I., Rihs, T.A., Becker, R., et al., 2014. Deviant dynamics of EEG resting state pattern in 22q11.2 deletion syndrome adolescents: a vulnerability marker of schizophrenia? Schizophr. Res. 157 (1–3), 175–181.

Van Amelsvoort, T.V., Daly, E., Robertson, D., et al., 2001. Structural brain abnormalities associated with deletion at chromosome 22q11: quantitative neuroimaging study of adults with velo-cardio-facial syndrome. Br. J. Psychiatry 178 (5), 412–419.

Van Amelsvoort, T., Daly, E., Henry, J., et al., 2004. Brain anatomy in adults with velocardiofacial syndrome with and without schizophrenia: preliminary results of a structural magnetic resonance imaging study. Arch. Gen. Psychiatry 61 (11), 1085–1096.

van den Heuvel, M.P., Fornito, A., 2014. Brain networks in schizophrenia. Neuropsychol. Rev. 24 (1), 32–48.

van den Heuvel, M.P., Sporns, O., 2011. Rich-club organization of the human connectome. J. Neurosci. 31 (44), 15775–15786.

van den Heuvel, M.P., Mandl, R.C.W., Stam, C.J., Kahn, R.S., Pol, H.E.H., 2010. Aberrant fron-
tal and temporal complex network structure in schizophrenia: a graph theoretical
analysis. J. Neurosci. 30 (47), 15915–15926.

van den Heuvel, M.P., Sporns, O., Collin, G., et al., 2013. Abnormal rich club organization
and functional brain dynamics in schizophrenia. JAMA Psychiatry 70 (8), 783–792.

van den Heuvel, M.P., de Reus, M.A., Feldman Barrett, L., et al., 2015. Comparison of diffu-
sion tractography and tract-tracing measures of connectivity strength in rhesus ma-
caque connectome. Hum. Brain Mapp. 36 (8), 3064–3075.

Wang, R., Benner, T., Sorensen, A., Wedeen, V.J., 2007. Diffusion toolkit: a software pack-
age for diffusion imaging data processing and tractography. Proc. Int. Soc. Magn.
Reson. Med. 15, 3720.

Wang, Q., Su, T.-P., Zhou, Y., et al., 2012a. Anatomical insights into disrupted small-world
networks in schizophrenia. NeuroImage 59 (2), 1085–1093.

Wang, J.Y., Abdi, H., Bakhadirov, K., Diaz-Arrastia, R., Devous, S., Michael, D., 2012b. A
comprehensive reliability assessment of quantitative diffusion tensor tractography.
NeuroImage 60 (2), 1127–1138.

Wechsler, D., 1991. Manual for the Wechsler Intelligence Scale for Children — Third Edi-
tion (WISC-III). The Psychological Corporation, San Antonio, TX.

Wechsler, D., 1997. Manual for the Wechsler Adult Intelligence Scale — Third Edition
(WAIS-III). The Psychological Corporation, San Antonio, TX.

Wolkin, A., Choi, S.J., Szilagyi, S., Sanfilipo, M., Rotrosen, J.P., Lim, K.O., 2003. Inferior frontal
white matter anisotropy and negative symptoms of schizophrenia: a diffusion tensor
imaging study. Am. J. Psychiatry 160 (3), 572–574.

Yu, Q., Sui, J., Rachakonda, S., et al., 2011. Altered topological properties of functional net-
work connectivity in schizophrenia during resting state: a small-world brain network
study. PLoS One 6 (9), e25423.

Zalesky, A., Fornito, A., Bullmore, E.T., 2010. Network-based statistic: identifying differ-
ences in brain networks. NeuroImage 53 (4), 1197–1207.

Zalesky, A., Fornito, A., Seal, M.L., et al., 2011. Disrupted axonal fiber connectivity in
schizophrenia. Biol. Psychiatry 69 (1), 80–89.

Zhang, Y., Lin, L., Lin, C.-P., et al., 2012. Abnormal topological organization of structural
brain networks in schizophrenia. Schizophr. Res. 141 (2–3), 109–118.